RSC Advances

ROYAL SOCIETY OF CHEMISTRY

www.rsc.org/advances

One-step calcination method for synthesis of mesoporous g-C_3N_4/$NiTiO_3$ heterostructure photocatalyst with improved visible light photoactivity

Hui Wang [a, b], Xingzhong Yuan [a, b *], Hou Wang [a, b], Xiaohong Chen [c], Zhibin Wu [a, b], Longbo Jiang [a, b], Weiping Xiong [a, b], Yaxin Zhang [a, b], Guangming Zeng [a, b]

a. College of Environmental Science and Engineering, Hunan University, Changsha 410082, P.R. China

b. Key Laboratory of Environment Biology and Pollution Control, Hunan University, Ministry of Education, Changsha 410082, P.R. China

c. Collaborative Innovation Center of Resource-Conserving & Environment-Friendly Society and Ecological Civilization, Changsha 410083, P.R. China

[*] Corresponding author at: College of Environmental Science and Engineering, Hunan University, Changsha 410082, PR China. Tel.: +86 731 88821413; fax: +86 731 88823701.
E-mail address: yxz@hnu.edu.cn (X.Z. Yuan)

Abstract

A novel g-C_3N_4/$NiTiO_3$ composite was fabricated by one-step calcination method using dicyandiamide, tetrabutyl titanate and nickel acetate as the precursor. The samples were characterized by scanning electron microscopy, X-ray diffraction, X-ray photoelectron spectroscopy, N_2 adsorption/desorption isothermal, UV-vis diffuse reflection spectroscopy and photoluminescence spectroscopy. It was indicated that the hybrids owned large surface area, mesoporous structure and improved visible light absorption. The optimal g-C_3N_4 content in g-C_3N_4/$NiTiO_3$ composite was 18.4 wt%, and corresponding visible-light removal rate for nitrobenzene was 0.0132 min^{-1}, about 1.6 times higher than that of pure $NiTiO_3$. The enhanced photocatalytic activity may be attributed to the large surface area, the stronger absorption in the visible region and the efficient electron-hole separation.

Keywords

g-C_3N_4; $NiTiO_3$; Visible-light; Nitrobenzene; Photocatalysis

1. Introduction

In recent years, carbon materials with graphite-like structure, such as graphene, carbon nitride, and boron carbonitride, have attracted considerable attention in energy storage, adsorption and catalysis[1-4]. Remarkably, the graphitic carbon nitride (g-C_3N_4), a novel metal-free polymeric semiconductor, has received extensive interests because of its superior photocatalytic performance[5]. The g-C_3N_4 was identified to be a prospective visible-light-responsive photocatalyst with the suitable band gap of 2.7 eV and high chemical stability. However, g-C_3N_4 could suffer limited low sunlight absorption, low quantum efficiency and high recombination rate, which might result in low photocatalytic activity[6, 7]. Various attempts have been introduced to improve the photocatalytic activity of g-C_3N_4, such as increasing the surface area[8], doping[9], serving as co-catalyst[10] and so on. Particularly, integrating g-C_3N_4 with other semiconductors to form heterojunctions was found to be a high effective and feasible strategy. Recently, our group has reported a novel g-C_3N_4/MIL-125(Ti) heterostructures which demonstrated enhanced visible light photocatalytic activities[11]. Furthermore, novel g-C_3N_4/Bi_2WO_6[6], g-C_3N_4/BiOCl[12], g-C_3N_4/SnO_2[13], g-C_3N_4/WO_3[14] and g-C_3N_4/ZnO[15] composites were developed and obtained enhanced visible-light photocatalytic activity. However, most composite photocatalysts were mainly prepared based on the multi-step method. Commonly, g-C_3N_4 monomer was firstly synthesized, and then the hybrids were formed by sol-gel[16], precipitation[17], hydrothermal method[18]. If the photocatalysts could be fabricated by a convenient one-pot method, the impact would be tremendous in more areas. Therefore, it was imperative to utilize one-step method to integrate g-C_3N_4 with other semiconductors

for the improved photocatalytic activity.

Nickel titanate ($NiTiO_3$) had an ilmenite structure in which both Ni and Ti mostly prefer octahedral coordination with alternating cation layers solely occupied by Ni and Ti[19]. It was reported that $NiTiO_3$ had a band gap of 2.18 eV and possessed good photocatalytic activity in removing organic pollutants under light irradiation[20]. However, the $NiTiO_3$, as an individual photocatalyst, was limited by the poor quantum efficiency because of its narrow band gap[21]. $NiTiO_3$-based heterojunctions have been obtained in attempt to reduce the recombination rate of charge carriers, and included $Ag/NiTiO_3$[22], $CdS/NiTiO_3$[23] and $Fe_3O_4/NiTiO_3$[24]. To the best of our knowledge, the report on coupling $NiTiO_3$ with the polymeric semiconductor g-C_3N_4 was still scarce.

In the present study, a series of novel g-$C_3N_4/NiTiO_3$ composites were obtained by one-step calcination method using dicyandiamide, tetrabutyl titanate and nickel acetate as the precursor. The photocatalytic activity of the as-prepared composites was detected by the removal of NB under visible light irradiation. Then, a possible removal mechanism was also proposed based on energy band positions and photoluminescence spectra.

2. Experimental

The g-$C_3N_4/NiTiO_3$ composites were synthesized through a thermal calcination at 550 °C using dicyandiamide, tetrabutyl titanate and nickel acetate as the precursor. For the specific sample preparation, characterization and photocatalytic test have been shown in the Experimental section in the Supporting Information. The as-prepared

g-C_3N_4/$NiTiO_3$ samples with expected g-C_3N_4 contents of 10.1, 18.4 and 27.3 wt% were labeled as CT1, CT3, CT5, respectively.

3. Results and discussion

3.1 Characterization of the catalyst

The size and morphology of the g-C_3N_4, $NiTiO_3$ and CT3 samples were examined by SEM analysis (Fig. 1). As displayed in Fig. 1a, pure g-C_3N_4 sample presented aggregated morphologies consisting of irregular block-based flakiness and particles[8]. The $NiTiO_3$ was primarily comprised of nanorods with diameters of 1-2 μm and length of around 4 μm (Fig. 1b). Fig. 1c revealed that the $NiTiO_3$ nanorods were decorated on the surfaces of g-C_3N_4. Moreover, the EDS of the CT3 sample confirmed the existence of C, N, O, Ti and Ni (Fig. 1d). From the EDS analyses, the ratio of Ti, Ni and O was about 1: 1: 3 in the CT3 sample. The elemental mapping images displayed the distribution of $NiTiO_3$ on the g-C_3N_4 surface (Fig. 1f), demonstrating the formation of g-C_3N_4/$NiTiO_3$ hybrids.

The XRD patterns of g-C_3N_4, $NiTiO_3$ and CT3 were exhibited in Fig. 2a. The diffraction peaks of pure $NiTiO_3$ at 2θ of 24.1°, 33.1°, 35.7°, 40.9°, 49.5°, 54.0°, 62.5° and 64.0° can be indexed as the (012), (104), (110), (113), (024), (116), (214) and (300) crystal planes of ilmenite $NiTiO_3$ (JCPDS no. 33-0960). The distinct peak at 27.4° was observed in g-C_3N_4 sample, which well matched with (100) diffraction planes (JCPDS 87-1526). Comparatively, the new peak emerged in the hybrid as compared with $NiTiO_3$ when g-C_3N_4 was introduced. The XRD pattern of the CT3 composite revealed two sets of diffraction peaks from both g-C_3N_4 and $NiTiO_3$,

indicating the presence of two components.

The chemical composition and electronic structure of CT3 were characterized by the X-ray photoelectron spectroscopy (XPS) measurements. High resolution spectrums of C 1s, N 1s, O 1s, Ti 2p and Ni 2p were described in Fig. 2. Fig. 2b showed the C 1s spectrum, the peak observed at 284.8 eV derived from sp^3 C-C bonds, while the other signal of C=N coordination appeared at 287.4 eV[13, 25]. From Fig. 2c, the N 1s peak at 396.0 eV can be representatively ascribed to the N bonded to Ti atoms in the form of Ti-N bands[11]. The signal at 400.2 eV corresponded to the N atoms sp^2-bonded to two coordinated carbon atoms (C=N-C), and the other contribution at 401.5 eV was responsible for the bridging nitrogen atoms $N\text{-}(C)_3$[26, 27]. As described in Fig. 2d, O^{2-} ions surrounded by Ti atoms showed a binding energy at 529.5 eV, and the peak appeared at 531.0 eV was assigned to O^{2-} ions in the surface oxygen deficient regions[28]. The Ti 2p spectrum (Fig. 2e) exhibited the binding energies at 458.0 eV for Ti $2p_{3/2}$ and 463.7 eV for Ti $2p_{1/2}$. The spin-orbit splitting value of 5.7 eV for Ti 2p was typical for Ti^{4+}[29]. The peaks at 855.2 eV and 872.8 eV were conformed to the Ni $2p_{3/2}$ and Ni $2p_{1/2}$ (Fig. 2f), respectively. The peak positions and the spin-orbit splitting value of 17.6 eV indicated the presence of Ni^{2+}[20, 29]. The XPS and SEM results revealed the formation of CT3 composite.

UV-vis diffusive reflectance spectra (UV-vis DRS) of g-C_3N_4/$NiTiO_3$ composites, pure g-C_3N_4 and $NiTiO_3$ indicated that all of them presented photoabsorption property from the UV to visible regions (Fig. 3). The absorption edge of the pure g-C_3N_4 was shorter than 460 nm, while that of the $NiTiO_3$ depicted a major absorption edge

around 550 nm. Compared with the single $NiTiO_3$, the g-C_3N_4/$NiTiO_3$ photocatalysts exhibited the similar absorbance edge, but extended the absorbance to the visible light region due to the existence of g-C_3N_4.The results implied that the visible light response of the photocatalysts was enhanced by introducing g-C_3N_4 into the $NiTiO_3$ and leaded to possible charge-transfer between the valence band of g-C_3N_4 and the $NiTiO_3$[30].

The N_2 adsorption-desorption isotherm was used to characterize the $NiTiO_3$, g-C_3N_4 and CT3 composite. As illustrated in Fig. S1a, the BET surface area of component g-C_3N_4 was 10 m^2 g^{-1}, and that of the pristine $NiTiO_3$ was 57 m^2 g^{-1}. Notably, the BET surface area of CT3 increased to 61 m^2 g^{-1}, indicating that the CT3 had more activity sites for NB adsorption, which was favorable for photocatalysis. The average pore size diameter was calculated to be 12 nm, 16 nm and 16 nm for g-C_3N_4, $NiTiO_3$ and CT3 (Fig. S1b), respectively. The mesoporous structure may be caused by the accumulation of $NiTiO_3$ nanoparticles and also the gas from the pyrolysis of the precursor[20].

3. 2 Photocatalytic activity of NB under visible lights

A representative organic pollutant NB, a primary absorption band at 268 nm, was implemented to evaluate the photocatalytic efficiency of as-prepared samples under visible light irradiation ($\lambda \geq 420$ nm). Fig. 4a reflected the photocatalytic removal (C/C_0) of NB in the presence of the g-C_3N_4/$NiTiO_3$ with various loading levels of g-C_3N_4, pure g-C_3N_4 and $NiTiO_3$. For pure $NiTiO_3$, only 62% NB was degraded after 2 h irradiation. It was noteworthy that with the

increase of g-C_3N_4 content, photocatalytic activity of the hybrids for NB removal exhibited a rise first followed by a decline, indicating that the concentration of g-C_3N_4 exerted profound influence on the photocatalytic activity. Particularly, when the proportion of g-C_3N_4 climbed to 18.4%, the g-C_3N_4/$NiTiO_3$ hybrid was detected to perform the highest photocatalytic activity and almost 80% NB was degraded in 2 h. Furthermore, this value is also higher than other photocatalysts in the same irradiation time, such as Ag-RGO[31], Ce_2S_3[32], co-doped TiO_2[33], CdS/ g-C_3N_4[34] and hydroxynaphthalene-modified TiO_2[35]. Notably, differences in conditions such as phase structure, NB concentration, photocatalyst dosages and light density may lead to the diverse catalytic performances. However, the photocatalytic activity decreased when the ratio of g-C_3N_4 exceeded 18.4%. This may be caused by the fact that the excessive g-C_3N_4 would hinder the electrons transferring from the g-C_3N_4 to $NiTiO_3$, and thus reducing its photocatalytic performance[15].

To quantitatively understand the reaction kinetics of the NB removal, the experimental data were fitted by applying the pseudo-first-order kinetics model as expressed by $-\ln(C/C_0)=kt$. Where k (min^{-1}) and t (min) were the apparent first-order rate constant and irradiation time, C_0 (mg/L) and C (mg/L) were the initial and remaining concentrations of NB at each time. The model fitting plots and the corresponding k values were shown in Fig. S2. The order of NB removal rate for as-prepared samples was CT3 (0.0132 min^{-1}) > CT1 (0.0119 min^{-1}) > mixed CT3 (0.0110 min^{-1}) > CT5 (0.0093 min^{-1}) > $NiTiO_3$ (0.0082 min^{-1}) > g-C_3N_4 (0.0074 min^{-1}). It was apparent that the g-C_3N_4/$NiTiO_3$ photocatalysts showed higher photocatalytic

activity for NB removal than that of pure $NiTiO_3$ and g-C_3N_4. The improved photocatalytic efficiency may be caused by the following factors: (i) the stronger absorption in the visible light region provided more electron-hole pairs; (ii) the porous heterojunction facilitated a fast electron transport, which was favorable for the efficient separation of photogenerated carriers.

3.3 Mechanism

Two materials with disparate conduction band (CB) and valence band (VB) redox energy levels can be implemented to promote photogenerated carrier mobility and enhance the efficiency of interfacial charge transfer[6]. The band gap positions (E_g) of $NiTiO_3$, g-C_3N_4 and CT3 were estimated to be 2.18 eV, 2.7 eV and 2.34 eV (inset of Fig. 3), according to $E_g = 1240/\lambda$, where λ is the wavelength (nm) of the absorption edge[13]. Moreover, the CB and VB potentials (E_{CB} and E_{VB}, respectively) were imputed by the empirical equation $E_{VB}=X-E^e+1/2E_g$ and $E_{CB}=E_{VB}-E_g$. Where X is the electronegativity of the semiconductor, E^e is the energy of free electrons on the hydrogen scale (about 4.5 eV)[36]. The calculated E_{CB} and E_{VB} of g-C_3N_4 were -1.13 and +1.57eV, and those of $NiTiO_3$ were +0.2 and +2.38 eV, separately. The schematic diagramof the photocatalytic process for g-C_3N_4/ $NiTiO_3$ composite was depicted in Fig. 4c. Considering the E_{CB} of g-C_3N_4 was more negative than that of $NiTiO_3$, the electrons were transferred from the CB of g-C_3N_4 to the CB of $NiTiO_3$. While the generated holes in the VB of $NiTiO_3$ spontaneously migrated to that of g-C_3N_4, leaving the holes behind. Since the standard redox potential $E^0(O_2/H_2O_2)$ (+0.682 V vs. NHE) was more positive than the CB potential of $NiTiO_3$, The large quantity of O_2

brought into the solution could inhibit the h^+/e^- recombination by efficiently scavenging the electrons in $NiTiO_3$, producing H_2O_2[14]. At the same time, the holes in the VB of g-C_3N_4 can react further with H_2O to generate abundant •OH radicals[6, 13]. These highly reactive •OH radicals was beneficial for the efficient photocatalytic removel of nitrobenzene[37]. The above process was described as the follows:

$$g\text{-}C_3N_4/NiTiO_3 + hv \rightarrow g\text{-}C_3N_4(e^- + h^+)/NiTiO_3(e^- + h^+) \quad (1)$$

$$g\text{-}C_3N_4(e^- + h^+)/NiTiO_3(e^- + h^+) \rightarrow g\text{-}C_3N_4(h^+)/NiTiO_3(e^-) \quad (2)$$

$$2e^- + O_2 + 2H^+ \rightarrow H_2O_2 \quad (3)$$

$$h^+ + H_2O \rightarrow {}^{\cdot}OH + H^+ \quad (4)$$

$${}^{\cdot}OH + NB \rightarrow \text{Other products} \quad (5)$$

To further investigate the effect of the g-C_3N_4 modification, PL spectroscopy were useful for revealing the separation efficiency of the photogenerated electrons and holes[38]. As shown in Fig. 4b, the PL spectrum of pure $NiTiO_3$ exhibited a strong emission among these observed samples, implying that it possessed the rapid recombination rate of electrons and holes. Compared with the pure $NiTiO_3$, the introduction of g-C_3N_4 hardly changed the position of emission peak, but rather reduced its relative intensity. This clearly illustrated that the recombination rate of photogenerated electron-hole pairs was inhibited in the hybrids, and thus enhanced the photocatalytic activity. Moreover, the recycling and stability test of CT3 for the photocatalytic removal of NB was depicted in Fig. S3. It can be apparently seen that the photocatalytic performance had no significant decrease after five cycles. Additional, the XRD (Fig.S3b) and SEM analysis (Fig.S4) of CT3 before and after

photocatalysis exhibited no obvious change even after 5th reuse. These results indicated that the g-C_3N_4/$NiTiO_3$ composites possessed excellent photocatalytic stability, which was significant for the practical applications.

4. Conclusions

A series of novel g-C_3N_4/$NiTiO_3$ composites with large surface area and mesoporous structure were obtained via a facile calcination method. The CT3 photocatalyst presented the highest visible light photocatalytic activity for NB removal. The corresponding removal rate was 0.0132 min^{-1} which was higher than that of pure g-C_3N_4 (0.0074 min^{-1}) and $NiTiO_3$ (0.0082 min^{-1}). The large BET surface area and mesoporous structure, the stronger absorption in the visible region and the efficient electron-hole separation were the main reasons for the improved photocatalytic performance. Besides, cyclic experiments indicated the photocatalysts possessed a reusability and stability towards NB removal. Hence, it can be concluded that the novel g-C_3N_4/$NiTiO_3$ composite was a promising candidate for water treatment.

Acknowledgments

The authors gratefully acknowledge the financial support provided by the National Natural Science Foundation of China (No. 71431006, 21276069).

Reference

1. Wang, H.; Yuan, X.; Zeng, G.; Wu, Y.; Liu, Y.; Jiang, Q.; Gu, S., *Adv. Colloid Interfac.*, 2015**, 221**, 41-59.

2. Byers, J. C.; Billon, F.; Debiemme-Chouvy, C.; Deslouis, C.; Pailleret, A.; Semenikhin, O. A., *ACS appl. Mater. Inter.*, 2012**, 4**, (9), 4579-87.

3. Qin, L.; Yu, J.; Kuang, S.; Xiao, C.; Bai, X., *Nanoscale*, 2012**, 4**, (1), 120-3.

4. Wickramaratne, N. P.; Xu, J.; Wang, M.; Zhu, L.; Dai, L.; Jaroniec, M., *Chem. Mater.*, 2014**, 26**, (9), 2820-2828.

5. Wang, X.; Maeda, K.; Thomas, A.; Takanabe, K.; Xin, G.; Carlsson, J. M.; Domen, K.; *Nat. mater.*, 2009**, 8**, (1), 76-80.

6. Ge, L.; Han, C.; Liu, J., *Appl. Catal. B: Environ.*, 2011**, 108-109**, 100-107.

7. Liu, W.; Wang, M.; Xu, C.; Chen, S., *Chem. Eng. J.*, 2012**, 209**, 386-393.

8. Wang, X.; Maeda, K.; Chen, X.; Takanabe, K.; Domen, K.; Hou, Y.; Fu, X.; Antonietti, M., *J. Am. Chem. Soc.*, 2009**, 131**, (5), 1680-1.

9. Li, J.; Shen, B.; Hong, Z.; Lin, B.; Gao, B.; Chen, Y., *Chem. Commun.*, 2012**, 48**, (98), 12017-9.

10. Chang, C.; Fu, Y.; Hu, M.; Wang, C.; Shan, G.; Zhu, L., *Appl. Catal. B: Environ.*, 2013**, 142-143**, 553-560.

11. Wang, H.; Yuan, X.; Wu, Y.; Zeng, G.; Chen, X.; Leng, L.; Li, H., *Appl. Catal. B: Environ.*, 2015**, 174-175**, 445-454.

12. Zheng, C.-z.; Zhang, C.-y.; Zhang, G.-h.; Zhao, D.-j.; Wang, Y.-z., *Mater. Res. Bull.*, 2014**, 55**, 212-215.

13. Zang, Y.; Li, L.; Li, X.; Lin, R.; Li, G., *Chem. Eng. J.*, 2014**, 246**, 277-286.

14. Katsumata, K.; Motoyoshi, R.; Matsushita, N.; Okada, K., *J. Hazard. Mater.*, 2013**, 260**, 475-82.

15. Lv, H.; Ji, G.; Yang, Z.; Liu, Y.; Zhang, X.; Liu, W.; Zhang, H., *J. Colloid Interface Sci.*, 2015**, 450**, 381-7.

16. Yang, S.; Zhou, W.; Ge, C.; Liu, X.; Fang, Y.; Li, Z., *RSC Adv.*, 2013**, 3**, (16), 5631.

17. Li, F.-t.; Xue, Y.-b.; Li, B.; Hao, Y.-j.; Wang, X.-j.; Liu, R.-h.; Zhao, J., *Ind. Eng. Chem. Res.*, 2014, 141205091652003.

18. Wang, W.; Cheng, H.; Huang, B.; Liu, X.; Qin, X.; Zhang, X.; Dai, Y., *J. Colloid Interface Sci.*, 2015**, 442**, 97-102.

19. Moghiminia, S.; Farsi, H.; Raissi, H., *Electrochim. Acta*, 2014**, 132**, 512-523.

20. Qu, Y.; Zhou, W.; Ren, Z.; Du, S.; Meng, X.; Tian, G.; Pan, K.; Wang, G.; Fu, H., *J. Mater. Chem.*, 2012**, 22**, (32), 16471.

21. Inceesungvorn, B.; Teeranunpong, T.; Nunkaew, J.; Suntalelat, S.; Tantraviwat, D., *Catal. Commun.*, 2014**, 54**, 35-38.

22. Lin, Y.-J.; Chang, Y.-H.; Chen, G.-J.; Chang, Y.-S.; Chang, Y.-C., *J. Alloy Compd.*, 2009**, 479**, (1-2), 785-790.

23. Qu, Y.; Zhou, W.; Jiang, L.; Fu, H., *RSC Adv.*, 2013**, 3**, (40), 18305.

24. Zhang, Y.; Gu, J.; Murugananthan, M.; Zhang, Y., *J. Alloy Compd.*, 2015**, 630**, 110-116.

25. Cao, S.-W.; Liu, X.-F.; Yuan, Y.-P.; Zhang, Z.-Y.; Liao, Y.-S.; Fang, J.; Loo, S. C. J.; Sum, T. C.; Xue, C., *Appl. Catal. B: Environ.*, 2014**, 147**, 940-946.

26. Huang, L.; Xu, H.; Zhang, R.; Cheng, X.; Xia, J.; Xu, Y.; Li, H., *Appl. Surf. Sci.*, 2013**, 283**, 25-32.

27. Cui, Y.; Zhang, J.; Zhang, G.; Huang, J.; Liu, P.; *J. Mater. Chem.*, 2011**, 21**, (34), 13032.

28. Song, G.; Chu, Z.; Jin, W.; Sun, H., *Chinese J. Chem. Eng.*, 2015.

29. Yang, G.; Chang, W.; Yan, W., *J. Sol-Gel Sci. Techn.*, 2013**, 69**, (3), 473-479.

30. Li, X.; Li, M.; Yang, J.; Li, X.; Hu, T.; Wang, J.; Sui, Y.; Wu, X.; Kong, L., *J. Phys. Chem. Solids*, **2014,** 75, (3), 441-446.

31. Qusti, A. H.; Mohamed, R. M.; Abdel Salam, M., *Ceram. Int.*, 2014**, *40***, (4), 5539-5546.

32. Chen, S.; Zhang, H.; Fu, X.; Hu, Y., *Appl. Surf. Sci.*, 2013**, *275***, 335-341.

33. Shen, X. Z.; Liu, Z. C.; Xie, S. M.; Guo, J., *J. Hazard. Mater.*, 2009**, *162***, (2-3), 1193-8.

34. Dai, X.; Xie, M.; Meng, S.; Fu, X.; Chen, S., *Appl. Catal. B: Environ.*, 2014**, *158-159***, 382-390.

35. Kamegawa, T.; Seto, H.; Matsuura, S.; Yamashita, H., *ACS appl. Mater. Inter.*, 2012**, *4***, (12), 6635-9.

36. Li, H.; Liu, J.; Hou, W.; Du, N.; Zhang, R.; Tao, X., *Appl. Catal. B: Environ.*, 2014**, 160-161**, 89-97.

37. Sun, Z.; Zhao, M.; Li, F.; Wang, T.; Xu, L., *Mater. Res. Bull.*, 2014**, 60**, 524-529.

38. Zhou, X.; Jin, B.; Chen, R.; Peng, F.; Fang, Y., *Mater. Res. Bull.*, 2013**, 48**, (4), 1447-1452.

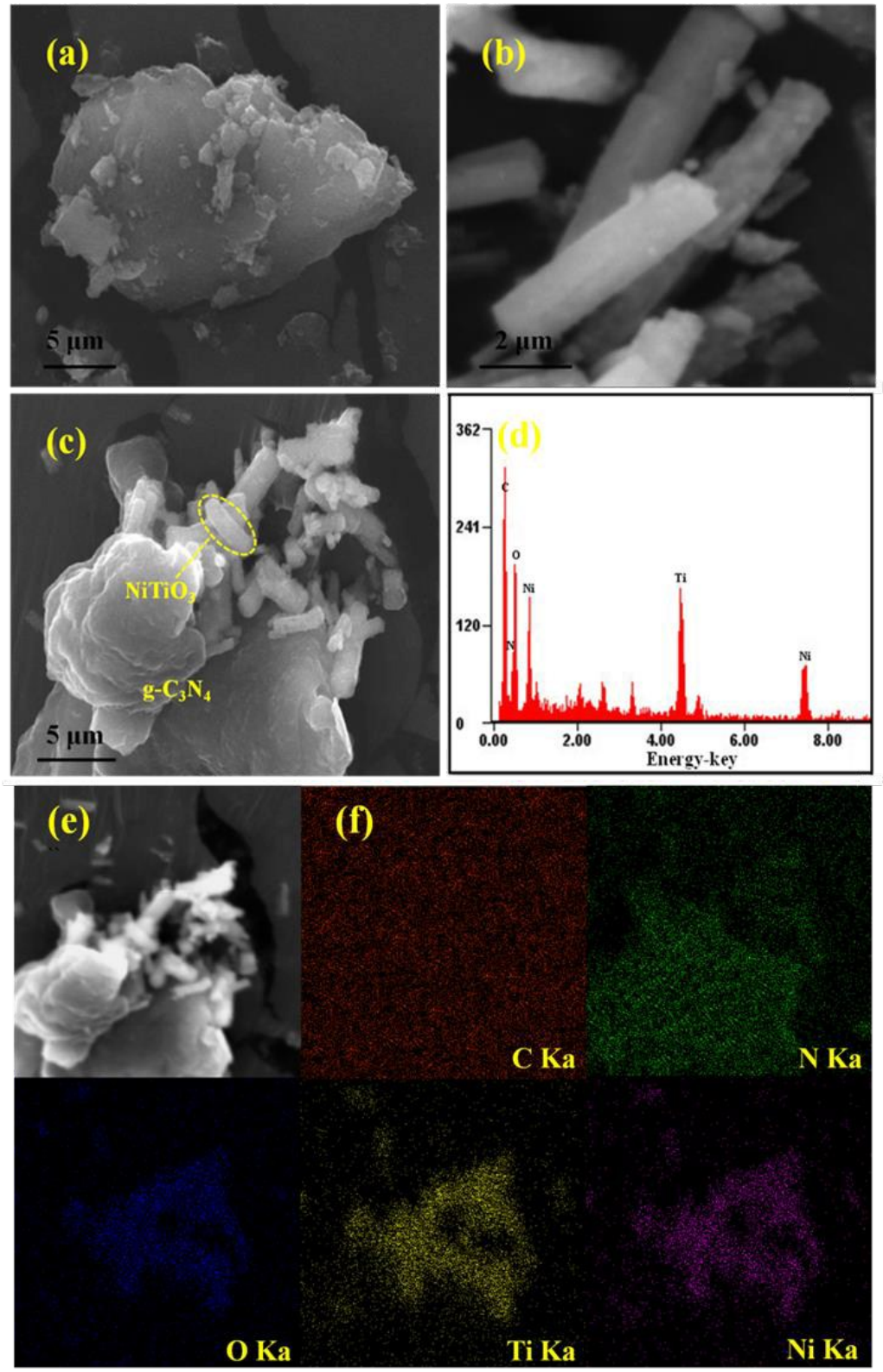

Fig.1. SEM images of (a) g-C_3N_4, (b) $NiTiO_3$, (c) CT3; (d) the EDX spectrum and (f) corresponding elemental mapping images of CT3.

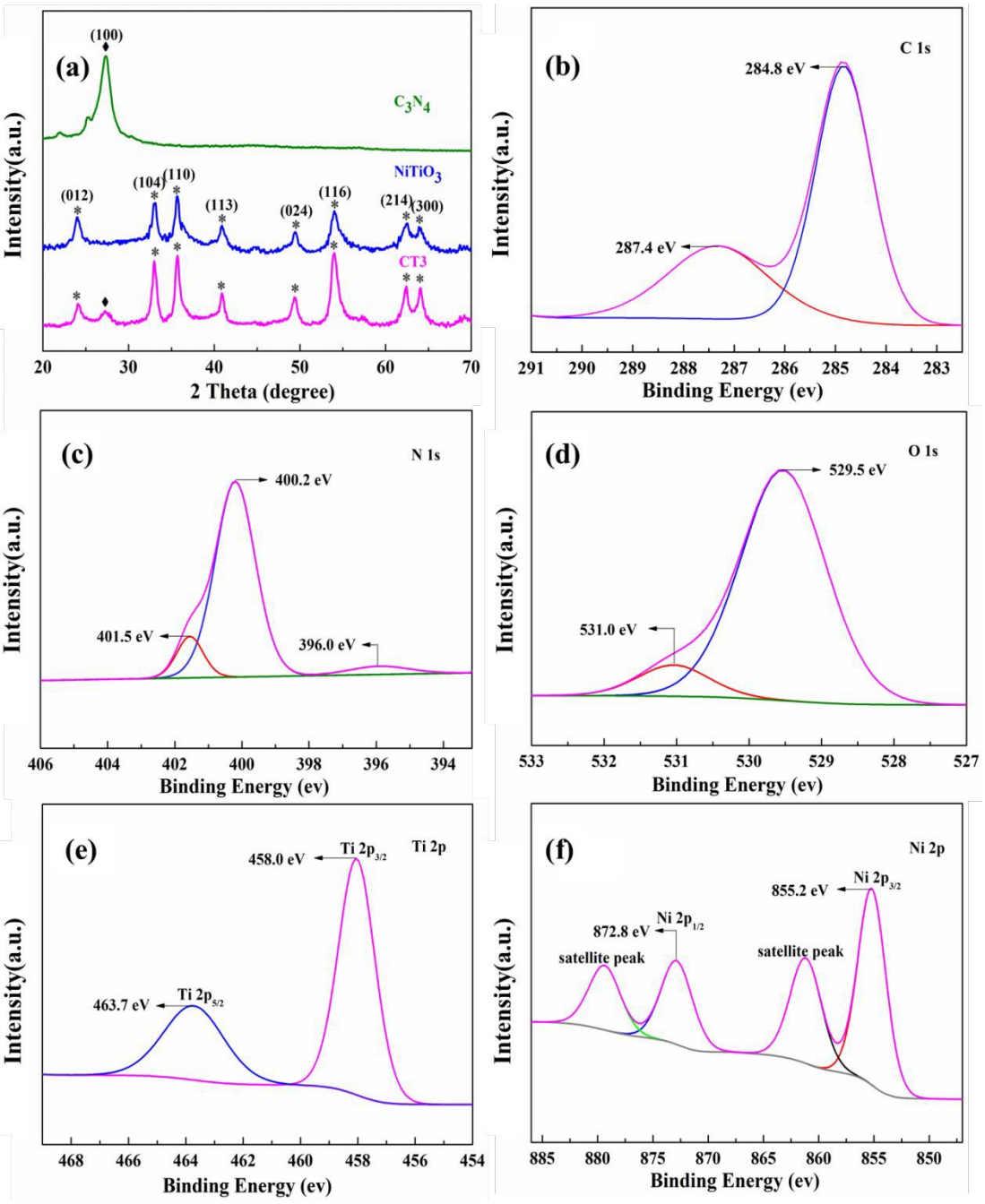

Fig.2. (a) XRD patterns of samples; and XPS spectra of CT3 (b) C 1s, (c) N 1s, (d) O 1s, (e) Ti 2p, (f) Ni 2p.

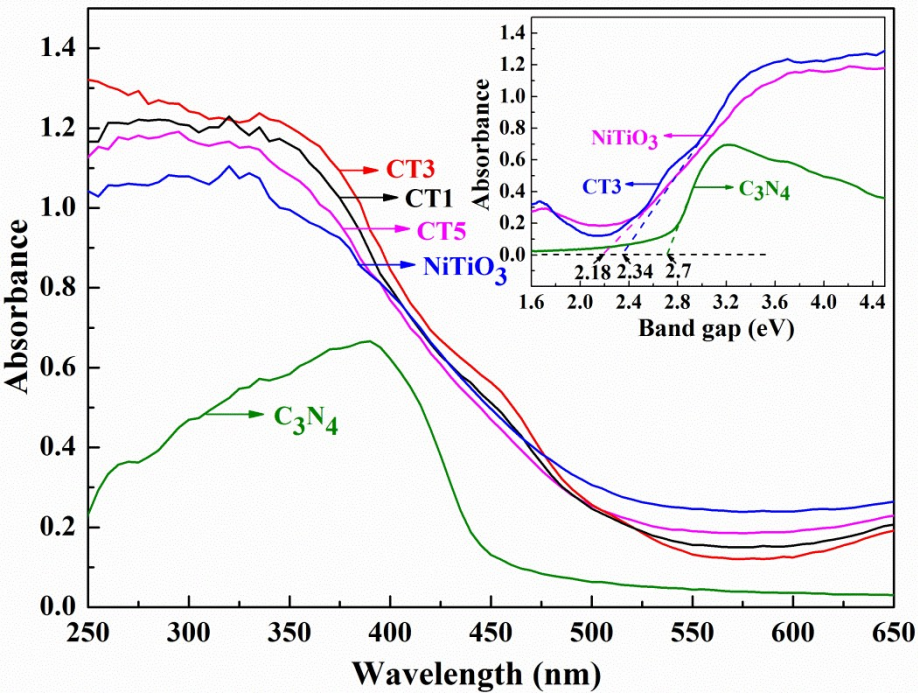

Fig.3. (a) UV-vis diffuses reflectance spectra of g-C_3N_4, $NiTiO_3$ and g-C_3N_4/$NiTiO_3$ composites.

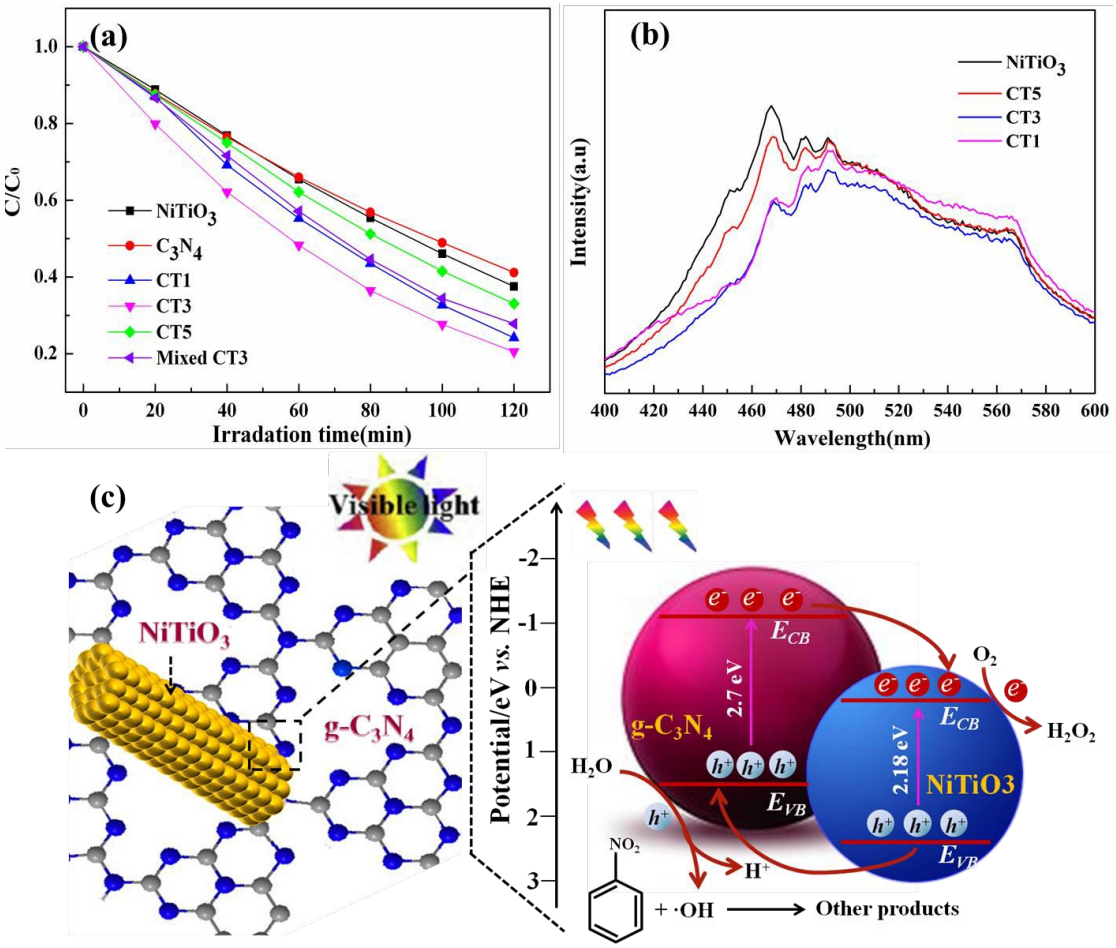

Fig.4. (a) Photocatalytic removel of NB over samples under visible light; (b) Photoluminescence spectra of g-C_3N_4/$NiTiO_3$ samples; (c) Proposed mechanism for the NB removel on the g-C_3N_4/$NiTiO_3$ composites under visible light irradiation.